



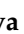




Article

Functionalized Microbial Consortia with Silver-Doped Hydroxyapatite (Ag@HAp) Nanostructures for Removal of RO84 from Industrial Effluent

Suriyaprabha Rajendran ¹, Virendra Kumar Yadav ^{2,*} , Amel Gacem ³ , Jari S. Algethami ⁴ , Mohammed S. Alqahtani ⁵ , Fahad M. Aldakheel ⁶ , Abdulkarim S. Binshaya ⁷, Nahed S. Alharthi ⁷, Imtiaz A. Khan ⁸, Saiful Islam ⁹, Yongtae Ahn ¹⁰  and Byong-Hun Jeon ^{10,*} 

- ¹ School of Nanosciences, Central University of Gujarat, Gandhinagar 302030, Gujarat, India; sooriyarajendran@gmail.com
 - ² Department of Biosciences, School of Liberal Arts & Sciences, Mody University of Science and Technology, Sikar 332311, Rajasthan, India
 - ³ Department of Physics, Faculty of Sciences, University 20 Août 1955, 26 El Hadaiek, Skikda 21000, Algeria; gacem_amel@yahoo.fr
 - ⁴ Department of Chemistry, College of Science and Arts, Najran University, P.O. Box 1988, Najran 11001, Saudi Arabia; jsalgethami@nu.edu.sa
 - ⁵ Department of Pharmaceutics, College of Pharmacy, King Saud University, P.O. Box 2457, Riyadh 11451, Saudi Arabia; msaalqahtani@ksu.edu.sa
 - ⁶ Department of Clinical Laboratory Sciences, College of Applied Medical Sciences, King Saud University, Riyadh 11433, Saudi Arabia; faldakheel@ksu.edu.sa
 - ⁷ Department of Medical Laboratory Sciences, College of Applied Medical Sciences, Prince Sattam Bin Abdulaziz University, Alkharj 21589, Saudi Arabia; abd.aldosari@psau.edu.sa (A.S.B.); n.alharthi@psau.edu.sa (N.S.A.)
 - ⁸ Department of Microbiology, Immunology and Tropical Medicine, George Washington University, Washington, DC 20037, USA; imti56@gwu.edu
 - ⁹ Civil Engineering Department, College of Engineering, King Khalid University, Abha 61421, Saudi Arabia; sfakrul@kku.edu.sa
 - ¹⁰ Department of Earth Resources & Environmental Engineering, Hanyang University, 222-Wangsimni-ro, Seongdong-gu, Seoul 04763, Korea; ytahn83@hanyang.ac.kr
- * Correspondence: bhjeon@hanyang.ac.kr (B.-H.J.); yadava94@gmail.com (V.K.Y.)



Citation: Rajendran, S.; Yadav, V.K.; Gacem, A.; Algethami, J.S.; Alqahtani, M.S.; Aldakheel, F.M.; Binshaya, A.S.; Alharthi, N.S.; Khan, I.A.; Islam, S.; et al. Functionalized Microbial Consortia with Silver-Doped Hydroxyapatite (Ag@HAp) Nanostructures for Removal of RO84 from Industrial Effluent. *Crystals* **2022**, *12*, 970. <https://doi.org/10.3390/cryst12070970>

Academic Editor: Jaime Gómez Morales

Received: 18 May 2022

Accepted: 7 July 2022

Published: 11 July 2022

Publisher's Note: MDPI stays neutral with regard to jurisdictional claims in published maps and institutional affiliations.



Copyright: © 2022 by the authors. Licensee MDPI, Basel, Switzerland. This article is an open access article distributed under the terms and conditions of the Creative Commons Attribution (CC BY) license (<https://creativecommons.org/licenses/by/4.0/>).

Abstract: Considering that freshwater is a necessity for human life, sewage treatment has been a serious concern for an increasing number of scientists and academics in recent years. To clean industrial effluents, innovative catalysts with good adsorption, chemical stability, and physicochemical properties have been constructed. Here, a prospective microbial consortium was extracted from the wastewater and used as a low-cost catalyst that was functionalized with silver and silver-doped hydroxyapatite (Ag@HAp) nanostructures made using a sonochemical approach. The structural, optical, and crystal phases of Ag and Ag-doped hydroxyapatite (Ag@HAp) nanostructures were studied using ultraviolet-visible (UV-Vis), Fourier transfer infrared spectroscopy (FTIR), X-ray diffraction (XRD), field emission scanning electron microscopy (FESEM), and high-resolution transmission electron microscopy (HRTEM) techniques. The degradation action of functionalized microbial consortia was examined against reactive orange 84 (RO84) organic discharge. Excellent efficiency for the removal of industrial effluents was found for the Ag NPs and Ag-doped hydroxyapatite (Ag@HAp) loaded with microbial consortia. A maximum of 95% of the decolorization properties of the RO84 dye were obtained in the case of microbial consortia with Ag and Ag@HAp, which was better than the consortia alone (80.32% for 5 ppm and 69.54% for 20 ppm). The consortia/Ag showed 93.34% for 5 ppm and 85.43% for 20 ppm, while was higher for consortia/Ag@HAp (95.34 and 88.43%). The use of these surface-modified nanocatalysts for wastewater treatment and waste effluents discharged from laboratories, the chemical industry, and other sources could be expanded.

Keywords: microbial consortia; Ag@HAp nanoparticles; surface modifications; industrial effluents; environmental applications

1. Introduction

The increased number of chemical industries and raw material manufacturers that discharge aromatic cyclic hydrocarbons as well as harmful byproducts or pollutants detected in wastewater have become serious problems nowadays [1,2]. The decomposition of azo organic dyes from wastewater has long been a significant environmental issue because many of these dyes are toxic to microorganisms and dangerous to humans. In this context, reactive orange 84 (RO84), one of the most popular dyes, is frequently employed for dyeing textile and inking paper, as well as for other commercial uses, such as the synthesis of toys, foods, and bulk drugs. Additionally, due to reactive dyes' water solubility, traditional biological, physical, and chemical methods fail to effectively clean dye discharge [3,4]. Therefore, researchers and employees have been inspired to develop effective green technologies to address such environmental challenges, particularly in the dye and textile sectors. Many studies have been conducted in the academic and industrial sectors to reduce the high organic and solid content of disposed wastewater [5,6]. Adsorption, membrane separation, physical and chemical coagulation, advanced oxidation processes (AOP), and biodegradation are some of the treatment methods that have been researched for use in treating wastewater. Due to its great performance and market viability, adsorption technologies are the most effective method for separating and removing dye molecules from wastewater [7,8]. Owing to the huge specific surface area, extensive active pores, low cost, and lack of toxicity, nanomaterials hold promise for having better adsorption performance. Hence to treat organic (heterocyclic/aromatic)-based wastes, several strategies, including photochemical, biological, and electrochemical processes, have been explored using desired nanocatalysts. Nanoparticles are readily available (speedy fabrication) and environmentally friendly (their production involves nontoxic building resources), and their potential for removing a particular azo dye merits further investigation. Nanoparticles also have the benefit of being usable in a pH range (neutral to basic) that is near to the pH of the dye industry effluent, requiring little to no pH modification. In addition, Ag NPs are advanced nanomaterials, especially encouraging for the removal of waste from the water, and can be easily manufactured from quite steady silver (I) salts. It has effective electron transport, with a late recombination rate in electrons and holes, and facilitates an advanced degradation quality towards aromatic organic substances from water [9,10]. Additionally, for the treatment of several dangerous substances that cannot be handled chemically, environmentally friendly nanoparticle synthesis is essential, and thus, researchers are particularly interested in developing Ag nanoparticle production techniques. The size and physicochemical features of silver nanoparticles significantly depend on the pH. Therefore, different sizes of Ag nanoparticles have been created and used for the photocatalytic activity of dye degradations and other environmental purposes [4,11]. In addition, potential microbes have been collected from wastewater and used to treat effluents in recent years. Selected adsorption and degradation features of specific microbial species have been explored for adsorbing heterocyclic organic dyes released from industrial sectors. However, the functionalized form of microbial consortia supported by nanostructures, such as homogenized Ag nanostructures, has been applied to enhance decolorization/removal efficiency in nanoscience and technologies. Notably, the adsorption properties of the catalysts are affected by the reaction parameters, including the reaction medium (pH), the amount of catalyst, and the nature of the targeted chemical contaminants or organic effluents [12,13]. Among the various chemical and biological catalysts, microbes combined with Ag NPs have been studied as efficient nanocatalysts, especially to remove organic toxic components from waste. It has been reported that biological resources have been employed as stronger catalytic substances associated with noble metal ions such as

Ag NPs [14,15]. The surface alteration of microbes and their use towards remediation have been found limited and significant for environmental concerns. Therefore, various efforts have been taken so far to make Ag NPs the most successful nanocatalysts by different additions of potential microbe species [16,17]. In this study, we firstly separated microbial consortia from the industrial effluents and studied their growth rate using Ag NPs and Ag-doped hydroxyapatite (Ag@HAp). The Ag@HAp microbial consortia were then used for the removal of RO84 dye discharged from industrial effluents. The impact of Ag@HAp microbial consortia at different concentrations (5, 10, and 20 ppm) and pH environments was studied for improving the decolorization/removal of RO84 dye.

2. Materials and Methods

The required chemicals, including silver nitrate, sodium borohydride, polyvinylpyrrolidone, ammonium dihydrogen phosphate, calcium nitrate, and ammonium hydroxide, were purchased from Sigma Aldrich, Bangalore, India. All reagents were of analytical grade.

2.1. Preparation of Silver Nanoparticles (Ag NPs)

The co-precipitation method was performed to synthesize the Ag NPs using a magnetic stirrer at 600 rpm at 25 °C for 4 h. AgNO₃ (0.01 M) was taken as a starting material and dissolved in 30 mL of distilled water. The surfactant PVP was added to prevent aggregation. Then, 0.01 M of NaBH₄ was added dropwise to the AgNO₃ solution at a low temperature. A change in color (pale yellow) indicated the presence of Ag NPs [9]. The magnetically stirred reaction solution was then centrifuged for 10 min at 6000 rpm at room temperature (2–3 times). The precipitate was obtained and carried out for the cleaning process. The obtained solid nanoparticles were washed with ethanol and dried at 25 °C. As a fine powder, the Ag NPs were used to determine the structural and morphological characterizations.

2.2. Silver-Doped Hydroxyapatite (Ag@HAp) NPs

AgNO₃ and Ca(NO₃)₂·4H₂O precursor salts were dissolved in deionized water to obtain a 300 mL Ca/Ag-containing solution. In addition, (NH₄)₂HPO₄ was dissolved in deionized water to make a 300 mL P-containing solution. The Ca/Ag-containing solution was stirred at 100 °C for 30 min. The pH of the P-containing solution was also adjusted to 10 with NH₃ and stirred continuously for 30 min. The P-containing solution was added drop by drop to the Ca/Ag-containing solution and stirred for 2 h, and the pH was constantly adjusted during the reaction. After the reaction, the deposited mixtures were washed several times with deionized water. The resulting material (Ag@HAp) was dried at 100 °C for 72 h and used for structural confirmation [18].

2.3. Growth Experiment of Consortia

The Ag and Ag@HAp were used to study the growth of the microbes present in the industrial effluent samples collected from Vatva, Ahmedabad, Gujarat, India. The samples underwent primary microbial characterization. First, the microorganisms were separated from the industrial effluent and identified. The identified microorganisms are shown in Table 1.

Table 1. List of microorganisms obtained from industrial effluents.

S. No.	Notation	Identified Organism	Accession Number NCBI
1	SP1	<i>Serratia liquefaciens</i>	Applied for accession
2	SP2	<i>Bacillus velezensis</i>	MH730069
3	SP3	<i>Achromobacter pulmonis</i>	Applied for accession
4	SP4	<i>Pseudomonas Stutzeri</i>	MH730067
5	SP5	<i>Pseudomonas Stutzeri</i>	MH730068
6	SP6	<i>Pseudomonas Stutzeri</i>	MH730066

2.4. Preparation of Consortia and Their Growth Test with Ag and without Ag@HAp

The isolated organisms were cultured together in nutrient agar broth. Then, 1 mL of each culture was taken and grown in sterilized nutrient broth. After incubation for one day, the cultured consortia underwent a growth test using Ag@HAp. The next day, the test organism cultures were transferred at a rate of 1% to 100 mL of nutrient broth kept in 250 mL conical flasks. Various concentrations of nanoparticles (50 ppm to 200 ppm of Ag and 50 ppm to 200 ppm of Ag@HAp) were carefully placed into each flask, leaving one as a control to track the normal growth of the microbial cells without nanoparticles. The experiments were performed using both a negative control (flask containing cells plus media) and positive control (flask containing nanoparticles plus media). The flasks were shaken at 180 rpm and 37 °C in a shaker incubator. Optical density measurements were taken every two hours from each flask to record the growth of the microbes in a spectrophotometer set at 600 nm. The growth rate of the microbial cells interacting with the nanoparticles was determined from a plot of the log of the optical density versus time. The experiment was performed in three sets to avoid errors.

2.5. Standardization of Dye Solution

The stock solution was prepared using 100 ppm, from which further concentrations were diluted and the standard preparation was performed. Before doing the remediation, the absorbance values were noted at λ 284 nm and λ 533 nm (absorbance wavelengths of RO84). The standard plot (Figure 1) of the concentration vs. the absorbance is shown, using the standard linear equation ($y = mx + c$), where Y = the absorbance at a particular wavelength, m = the slope of the plot, and x = the concentration that has to be obtained, c = the intercept of the slope.

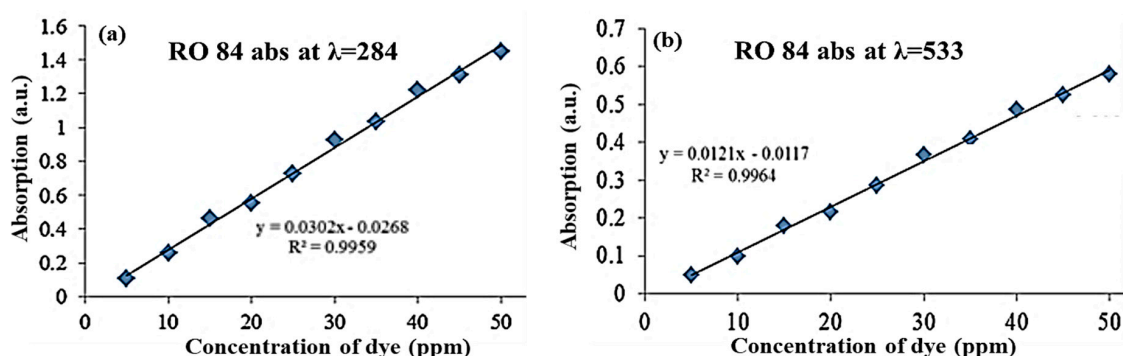


Figure 1. Absorption vs. concentration plot of RO84 dye at $\lambda = 284$ nm (a) and $\lambda = 533$ nm (b).

2.5.1. Remediation Experiment

Various concentrations of the dye solutions (5, 10, and 20 ppm in 100 mL) were added to a 250 mL conical flask with nutrient broth media. Consortia cultures with Ag and Ag@HAp were obtained after performing the growth experiment and added to the media (1% in 100 mL). The flask that had only consortia (without Ag and Ag@HAp) and dye solution and the flasks containing consortia with Ag and Ag@HAp at various concentrations were shaken at 180 rpm at room temperature for 5 days. Aliquots (2 mL) were obtained and a decolorization study was carried out at intervals of every 24 h at the wavelength corresponding to RO84. The experiment was carried out in 3 sets to avoid errors. The formulas used for calculating the decolorization are as follows:

$$\text{Decolorization\%} = (\text{Initial Conc} - \text{Final Conc}) / \text{Initial Conc} \times 100$$

Initial Conc—Initial concentration of dye calculated from the standard (at 0 h)

Final Conc—Final concentration of dye with respect to dye from the standard (at x h)

Whereas, x h = concentration calculated at uniform time intervals.

2.5.2. Effect of pH

Changes in the pH of a growth medium result from a change in the decolorization of reactive dyes. Bacteria are active in a wide range of pH values [18]. Reactive dyes bind to the cotton fiber under alkaline conditions so the decolorizing bacteria must be pH-tolerant. In this study, the decolorization study on the effect of pH was performed using pH levels of 3, 4, 5, 6, 7, and 8 over 5 days (in 20 ppm dye) with the help of a UV spectrometer.

2.6. Characterization Techniques

The techniques used for the characterizations were UV-Vis spectroscopy (Spectro 2060 plus spectrophotometer from 200–800 nm, with a 1-cm path length quartz cuvette) for the optical properties, and X-ray diffraction (XRD; Bruker, Germany, $\lambda = 0.15408$ nm, acceleration voltage of 40 kV, the scanning rate of $0.02^\circ/\text{s}$) for the structural phases. The structural morphology and elemental composition were identified using field emission scanning electron microscopy (FESEM; model JSM-7800F from JEOL) and high-resolution transmission electron microscopy (HR-TEM; JEOL JEM 2100F microscope operating at 170 kV) in conjunction with EDX, while the characteristic vibrational modes were identified for the expected functional groups using Fourier transform infrared spectroscopy (FTIR; Perkin Elmer) in the $400\text{--}4000\text{ cm}^{-1}$ range, at a resolution of 4 cm^{-1} , with 32 scans. The particle size distribution was examined using dynamic light scattering (DLS; Microtrac Zetatrac, U2771, DLS XE-70, Park System equipment) at RT with a set 1.5 cp liquid viscosity and 1.359 refraction index [19,20].

3. Results and Discussions

3.1. Structural Confirmations: XRD Analysis

Figure 2a,b describes the XRD patterns of the Ag NPs and Ag@HAp NPs. JCPDS reference no. 07-1167 confirms the presence of Ag NPs from the distinguishing peaks of (111), (220), (311), and (222), corresponding to FCC crystalline at diffraction angles of 38.15° , 44.39° , 64.59° , and 77.41° in Figure 2a [18,21]. The crystalline size of the Ag NPs was determined to be around 33.7 nm using the Scherrer Equation (1):

$$D = \frac{K\lambda}{\beta \cos \theta} \quad (1)$$

where D denotes the crystalline size of the Ag NPs, β indicates the full width at half-length maximum (FWHM) in radians, λ signifies the X-ray wavelength (1.5406 \AA), θ stands for the Bragg diffraction angle, and k is the Scherrer constant (0.9). Crystallographic peaks of Ag@HAp occurred at (1 0 0), (0 0 2), (2 1 1), (1 1 2), (3 0 0), (2 1 2), (2 1 3), and (0 0 4) in the XRD profile (JCPDS pattern no. 72-1243), as shown in Figure 2b [22]. The peaks were found to match the relevant standard JCPDS. The development of the Ag_3PO_4 phase specified the Ag^+ replacement for Ca^{2+} ions [23,24] and, likewise, proposed the electro-neutrality suitability of Ag^+ and PO_4^{3-} ions in HAp arrangement.

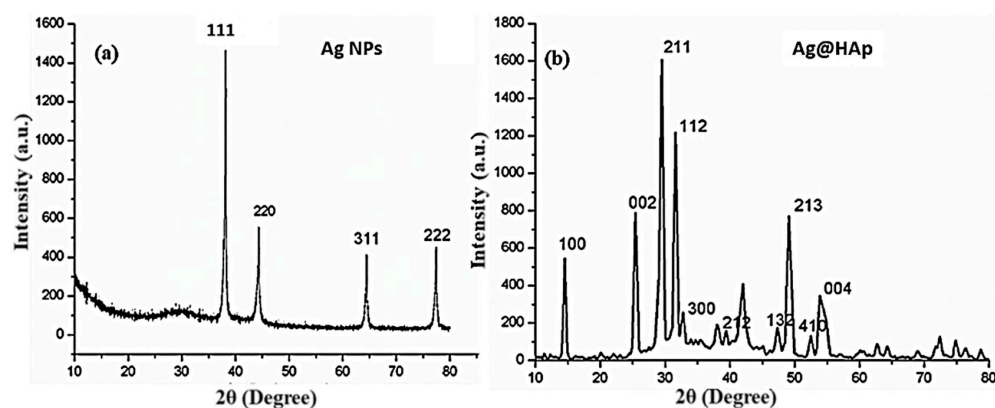


Figure 2. XRD profile: (a) XRD pattern of Ag NPs, (b) Ag@HAp NPs.

3.2. UV-Vis Absorbance Spectra

Figure 3 depicts the UV spectra of the synthesized silver nanoparticles, and the absorbance of the Ag NPs can be observed. Metal nanoparticles with unrestricted electrons tend to yield an SPR absorption band, owing to the shared vibration of the electrons of metal nanoparticles in resonance with electromagnetic waves [24]. The formation of the peak at around 420 nm displays the characteristics of the SPR of Ag NPs, which confirms the formation of Ag NPs [25].

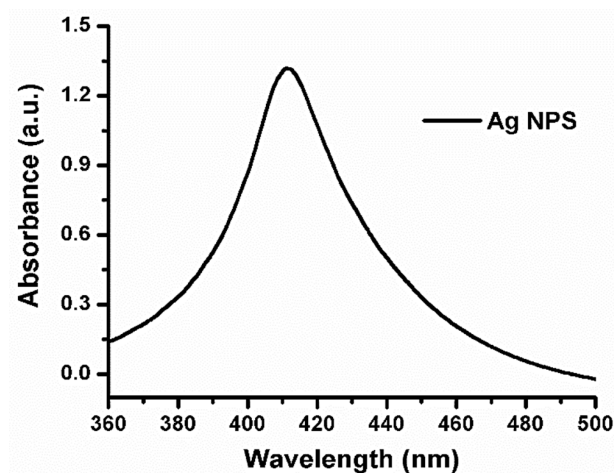


Figure 3. UV-Vis spectra of Ag NPs.

3.3. Functional Group Confirmations: FTIR Analysis

After the initial confirmation, the as-synthesized Ag and Ag@HAp NPs were further confirmed with FTIR spectra, as shown in Figure 4a,b. The FTIR spectrum confirms the presence of a few characteristic vibronic frequencies related to the attached functional groups of Ag and Ag@HAp. The peak detected at 571 cm^{-1} is attributed to the functional group of phosphate (PO_4^{3-}) of the HA [26]. The position of the band at 1075 cm^{-1} reflects the modes of the P-O stretching vibrations. The comprehensive peak at 3458 cm^{-1} is connected to the occurrence of the -OH group, possibly later than that of adsorbed water. However, following the addition of the Ag NPs, the O-H of H_2O molecules vanished. This outcome proposes that the Ag@HAp collaboration produced variations in the arrangement of the Ag@HAp nanostructures. This structural modification can be accredited to the replacement of Ag^0 (Ag NPs) with Ca^{2+} (HAp), as previously reported [22].

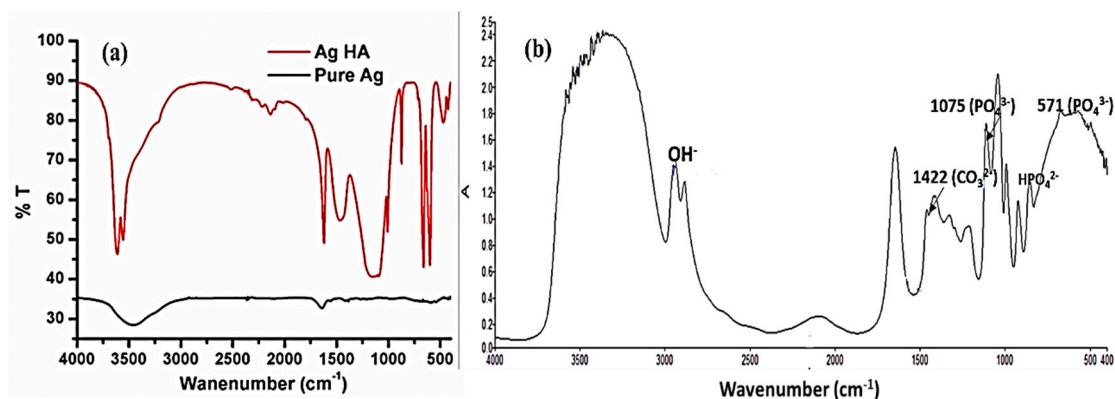


Figure 4. FTIR spectra of (a) Ag and (b) Ag@HAp nanoparticles.

3.4. Morphological Studies: HRTEM Analysis

Figure 5 shows the FESEM and HRTEM images, and EDAX with the SAED pattern of synthesized Ag NPs [27]. From the results obtained, it can be seen that the nanopar-

ticles have a spherical shape (Figure 5b), with the crystallographic spacing found to be 0.26 nm ($d_{(111)}$) for the Ag (Figure 5c). The solid crystal phase of the Ag particles was obtained from the SAED pattern, as shown in Figure 5d, with an average size of 10.6 nm (Figure 5e), revealing the Ag crystalline structure. The existing percentage of Ag is high in the EDAX graph (Figure 5f), which confirms the presence of Ag nanoparticles at a higher concentration.

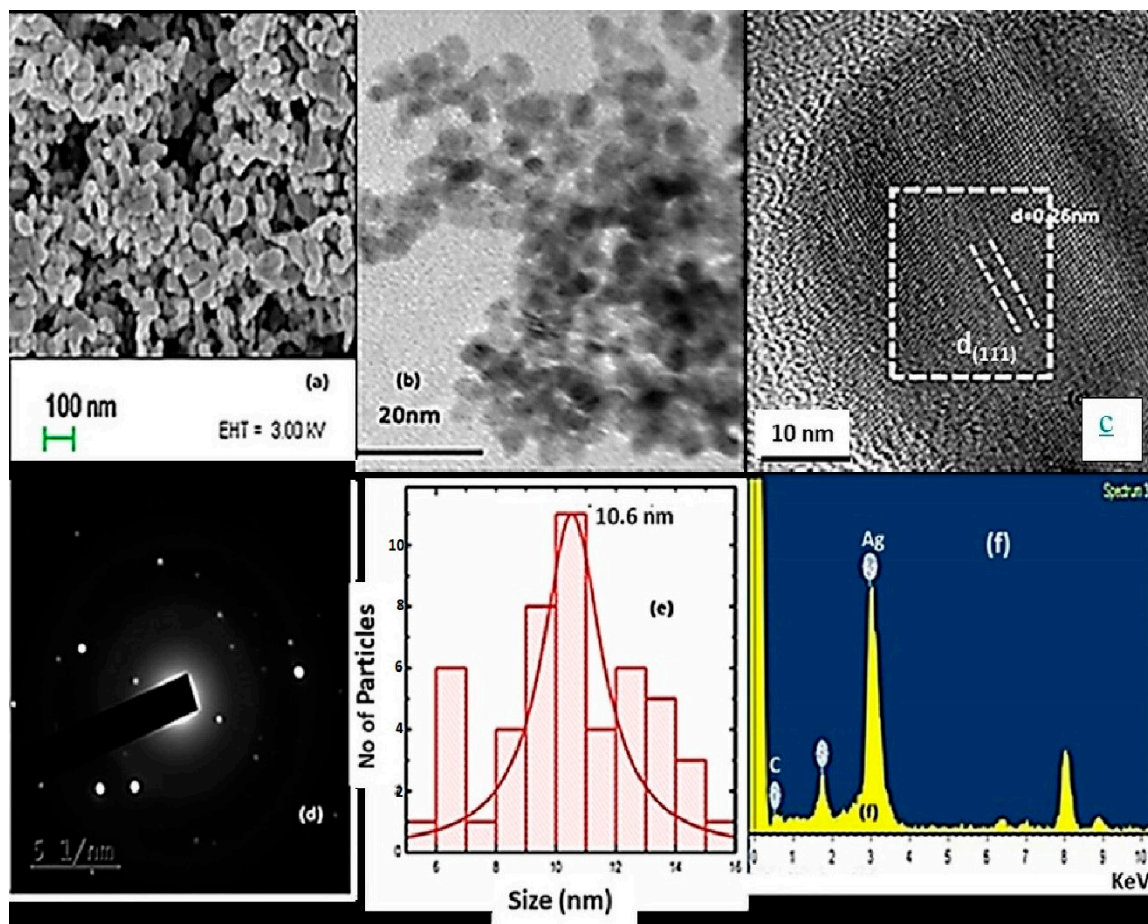


Figure 5. (a) FESEM and (b,c) HRTEM images. (d) SAED, (e) size distribution histogram, and (f) EDAX pattern of Ag NPs.

Figure 6 illuminates the TEM image of Ag@HAp, clearly showing the doping of Ag on the surface of HAp. The longer rod-like image confirms the presence of HAp, and the Ag was spotted in the matrix. The EDX pattern confirms the elemental amount of Ag@HAp where the presence of Ca, O, and P was expected. The histogram confirms the average size of the nanoparticle, which is around ≈ 12.5 nm.

3.5. DLS Study

To confirm the particle distribution of the Ag and Ag@HAp, DLS (Microtrac Zetatrac, U2771, DLS XE-70, Park System equipment) studies were carried out at RT. The bar graph shows a clear particle distribution of the Ag NPs (Figure 7a), ranging from 7 to 13.5 nm in size ($PDI \leq 1$). In the case of Ag@HAp, it shows comparably large sizes, ranging from 48 to 110 nm, as it covered the hydrodynamic radius, along with the Ag NP-doped HAp (Figure 7b).

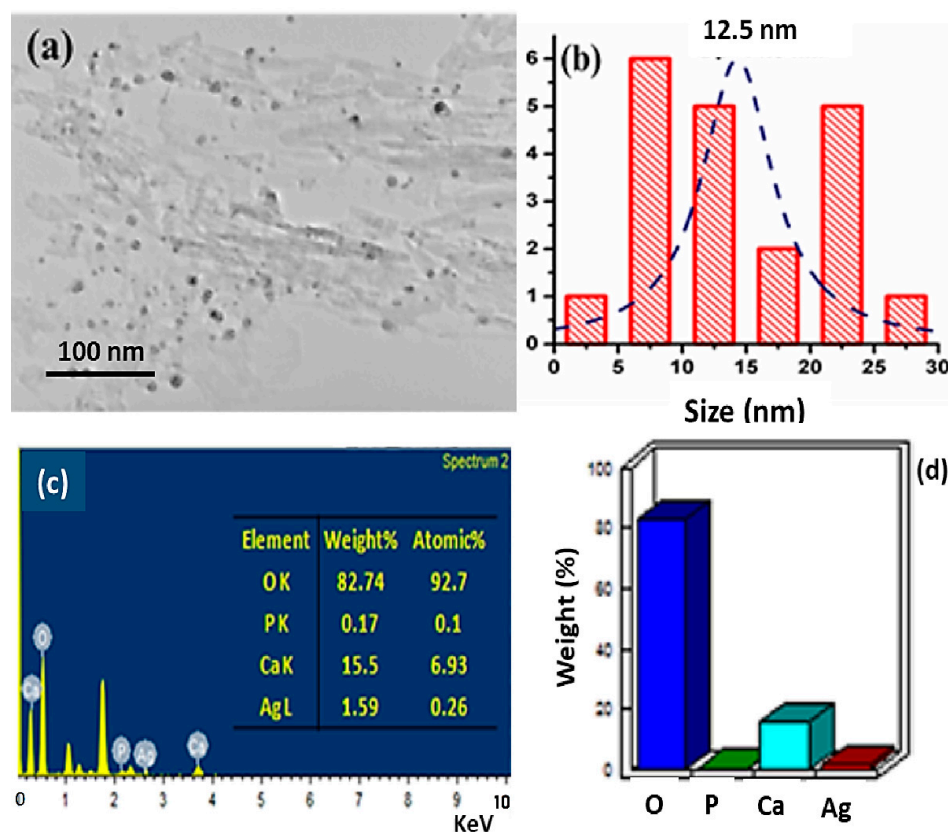


Figure 6. (a) TEM images, (b) histogram, (c) quantity analysis of Ag@HAp nanoparticles, and (d) weight % bar pattern.

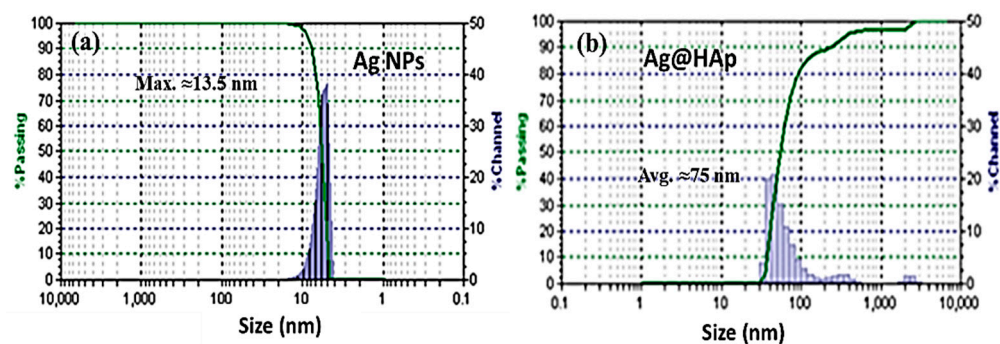


Figure 7. Particle size distribution pattern using DLS: (a) Ag NPs, and (b) Ag@HAp.

4. Remediation of Industrial Effluents

4.1. Removal of Microbial Pathogens

For several decades, nanomaterials such as silver, titanium, and zinc have been studied for their use in the disinfection of various waterborne disease-causing microorganisms due to their charge capacity. The present study aimed to obtain the antimicrobial properties of synthesized Ag and Ag@HAp nanoparticles. The exact mechanism of Ag NPs in the removal of pathogens is not clearly understood. It may be due to the cation (Ag^+) interaction with the donor groups of biological molecules, exhibiting antimicrobial activity. Therefore, there is a need for the embedment of Ag ions on the surface of biomaterials. Hence, ceramic materials play a vital role in this application. Nanoparticles were used to study the growth of isolated microbes from industrial wastewater [23]. Various concentrations of nanomaterials were introduced to the consortia of the microbes, and their growth was observed. The concentrations at which microbial growth was not inhibited were found to adsorb the nanoparticles in their growth. Hence, the nanoparticles adsorbed by the consortia were used to remove textile dye compounds.

4.2. Adsorption of Consortia by Nanoparticles

Several studies have demonstrated that Ag NPs show efficient antibacterial activity against microorganisms [15,17]. To obtain increased adhesion to microbes, there is a need for biodegradable polymers, with the support of Ag NPs to make them more efficient. Hydroxyapatite (HAp), along with Ag NPs, shows increased antimicrobial activity, which was synthesized via the coprecipitation method. The increased concentrations of both Ag and Ag@HAp resulted in the inhibition of microbial growth. Figure 8 exhibits the growth curve of the microbial consortia in the presence of Ag and Ag@HAp NPs.

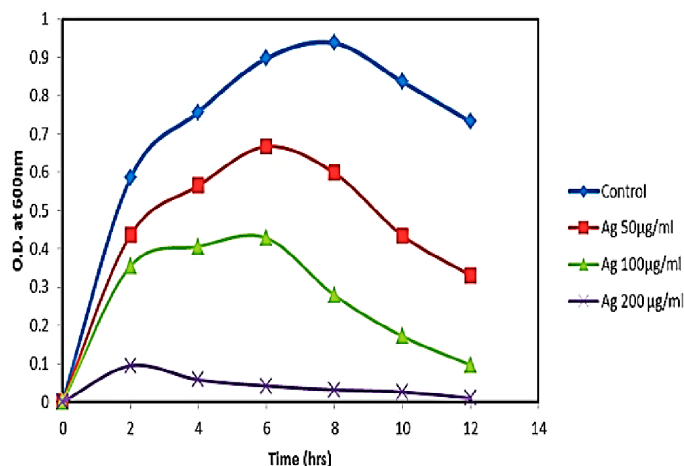


Figure 8. Growth studies of consortia at different concentrations of Ag NPs.

The growth of the microbial consortia was observed in the presence and absence of Ag and Ag@HAp nanoparticles at different concentrations (50 ppm, 100 ppm, and 200 ppm). In the absence of nanoparticles, the growth of the consortia was observed to be high at 12 h, whereas the presence of Ag and Ag@HAp (Figures 8 and 9) decreased the growth of the consortia because of their antimicrobial properties [22,23]. The growth curve of the consortia indicates two aspects—the antimicrobial properties of the nanoparticles and the ability of the consortia to adsorb the nanoparticles and grow in their presence. The study clearly shows that increased concentrations of nanoparticles inhibited the growth of microbes completely, while at limited concentrations, the consortium adsorbed the Ag and Ag@HAp and continued to grow. Up to 100 ppm, the growth was identical, whereas, above that concentration (200 ppm), there was no growth of bacteria. Hence, the consortia adsorbed the maximum number of nanoparticles at 100 ppm and they were used for the remediation of reactive dye RO84 by optimizing the pH conditions [28].

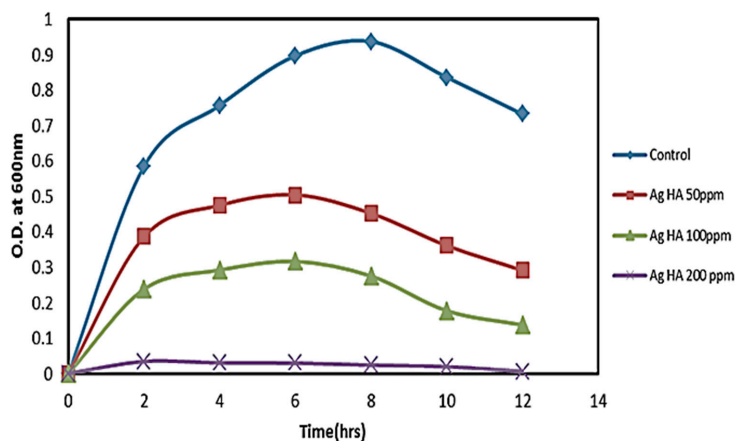


Figure 9. Growth curve of consortia at different concentrations of Ag@HAp.

5. Remediation of Reactive Orange 84 (RO 84)

Degradation of RO84

Before performing remediation, various concentrations of dye solutions were prepared from the stock solution (100 ppm), and their absorbance was observed at the respective wavelengths ($\lambda = 284$ and 533 nm). The standard graph is shown in Figure 10a–c.

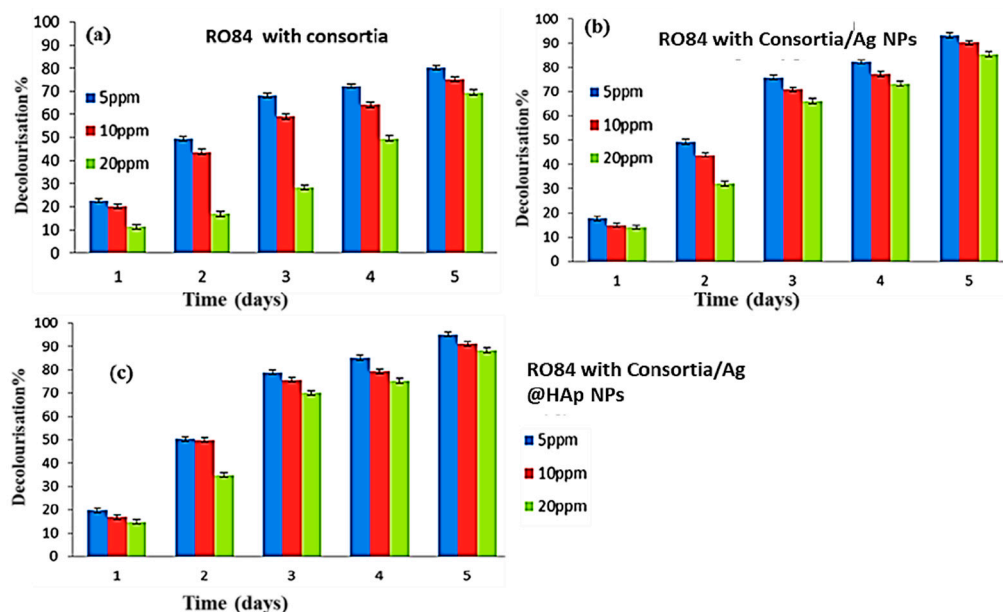


Figure 10. (a) Decolorization % of RO84 with only consortia, (b) with consortia and Ag, and (c) consortia and Ag@HAp.

The microbial consortia alone and the microbial consortia with nanoparticles were used for the degradation of RO84. The decolorization was measured at a visible wavelength of 533 nm. The concentration was calculated, and the percentages of decolorization without nanoparticles and with nanoparticles are explained in Figure 10a–c, respectively.

The decolorization process performed with consortia alone showed 80% decolorization for a minimum concentration of 5 ppm, while it was found to be 69% for a maximum 20 ppm concentration of RO84 dye. The consortia with both the nanoparticles exhibited 93–95% decolorization with a 5-ppm concentration of RO84. At a maximum concentration of 20 ppm, it reached 85–88% in five days (Table 2). The consortia with both Ag and Ag@HAp did not show a significant difference in the decolorization because both had the almost same concentration of Ag. It would probably show a difference if the concentration of HAp changed [29,30]. The increased dye decolorization percentage found may have been due to the use of Ag and Ag@HAp. The combined properties of the Ag NPs and the remediating capability of the consortia increased the decolorization in comparison to the decolorization via the consortia alone.

Table 2. Decolorization % of dye (5–20 ppm) by consortia alone and consortia with nanoparticles.

Samples	5 ppm	10 ppm	20 ppm
Consortia	80.32	75.45	69.54
Consortia/Ag	93.34	90.19	85.43
Consortia/Ag@HAp	95.34	91.20	88.43

Figure 11 shows the decolorization patterns at different pH levels. The species in the consortia were capable of surviving in an alkaline pH in comparison to an acidic pH (3–5). An increase in decolorization was noticed with changes in the pH (6–8). The growth was found to be higher with a pH of 5.5 or more; the bacterial consortia were adsorbed and

the maximum decolorization percentage reached 63–72%. The consortia were found to be efficient in the case of an alkaline pH, increasing the decolorization of the textile dye compounds at a pH of 6–8 (Table 3) [31]. It can be concluded that the buffering qualities and surface charge of HAp were the result of the acid-base interactions of the reactive surface sites since they displayed amphoteric abilities and functioned as a buffer in a fairly wide pH range. Ag NP-doped HAp produced negatively charged OH ions (Equation (2)), felicitating a favorable pH condition for the removal of the dye. The metallic Ag NPs had an electron transport ability to interact with the azo group of the dyes as the azo group had excess electrons.

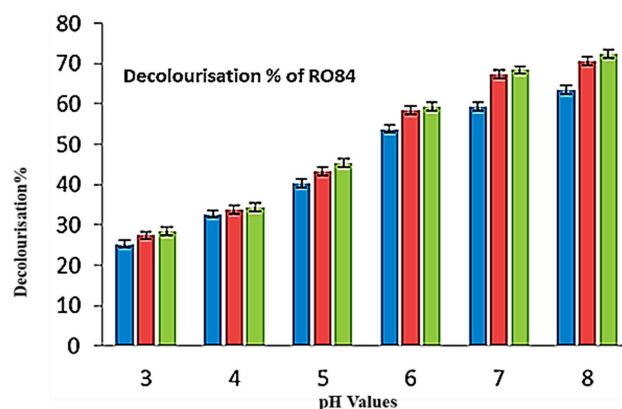
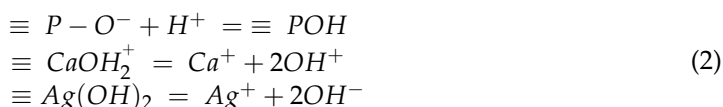


Figure 11. Decolorization percentage of RO84 at different pH levels.

Table 3. Decolorization % RO84 at different pH levels (3–8).

pH	Consortia	Consortia/(Ag)	Consortia/(Ag: HA)
3	25.33	27.43	28.54
4	32.73	33.76	34.34
5	40.35	43.34	45.35
6	53.85	58.54	59.43
7	59.34	67.46	68.43
8	63.47	70.67	72.36

Using effective metal and metal-based nanocatalysts, environmental difficulties, such as wastewater cleaning, dye remediation, and heavy metal elimination, have been resolved [32–34]. Due to the outstanding potential of hybrid nanostructures for medicinal, optoelectronic, and environmental applications, numerous academic and scientific studies have been conducted to create effective and affordable nanocatalysts [35–38].

6. Conclusions

We used promising microbial consortia as inexpensive nanocatalysts that were functionalized with silver and Ag@HAp nanostructures utilizing the sonochemical method. The morphological and compositional characteristics of the as-prepared Ag and Ag@HAp nanomaterials were confirmed using the UV-Vis, FTIR, XRD, FESEM, HRTEM, and DLS techniques. An SPR band at around 420 nm confirmed the formation of Ag NPs, which was further confirmed by XRD (FCC crystalline phase with a maximum crystal size of 33.7 nm). The HRTEM results show almost spherical-shaped Ag NPs, with 10.6 and 12.5 nm Ag and Ag@HAp structures. The ability of functionalized microbial consortia to adsorb reactive orange 84 (RO84) organic effluent was examined. For industrial effluents, Ag NPs and Ag@HAp loaded with microbial consortia showed good RO84 removal properties. The

maximum 95% decolorization properties of the RO84 dye were obtained in the case of the microbial consortia with Ag and Ag@HAp, which was better than the consortia alone (80.32% for 5 ppm and 69.54% for 20 ppm). The consortia/Ag showed decolorization of 93.34% at 5 ppm and 85.43% at 20 ppm, while it was higher for the consortia/Ag@HAp (95.34 and 88.43%). The wastewater and waste effluents from the chemical sector and laboratories could be cleaned up using these surface-modified nanocatalysts.

Author Contributions: Conceptualization, S.R., N.S.A., A.S.B. and B.-H.J.; data curation, A.S.B., S.I., J.S.A. and Y.A.; methodology, M.S.A., F.M.A., S.I. and V.K.Y.; validation, J.S.A., M.S.A. and V.K.Y.; formal analysis, V.K.Y., I.A.K., J.S.A. and A.G., resources, A.G., Y.A. and S.I.; writing—original draft preparation, S.R., N.S.A. and A.S.B., writing—review and editing, S.R., J.S.A., F.M.A., A.S.B., M.S.A., A.G., I.A.K. and B.-H.J.; supervision, N.S.A., A.G., Y.A. and V.K.Y.; project administration S.R., V.K.Y., F.M.A., J.S.A. and B.-H.J.; funding acquisition, B.-H.J., S.I., J.S.A. and I.A.K.; investigation, S.R., N.S.A., J.S.A. and F.M.A., software, S.R., J.S.A., Y.A. and N.S.A.; visualization, M.S.A., J.S.A., I.A.K., B.-H.J. and A.S.B. All authors have read and agreed to the published version of the manuscript.

Funding: This work was supported by the National Research Foundation of Korea (NRF) grant funded by the Korean government (MSIT) (2022R1C1C2003376). The authors also extend their appreciation to the Researchers Supporting Project, number RSP2022/R506, at King Saud University, Riyadh, Saudi Arabia for funding this work.

Institutional Review Board Statement: Not applicable.

Informed Consent Statement: Not applicable.

Data Availability Statement: Not applicable.

Conflicts of Interest: The authors declare that they have no conflict of interest.

References

1. Algethami, J.S.; Hassan, M.S.; Alorabi, A.Q.; Alhemiary, N.A.; Fallatah, A.M.; Alnaam, Y.; Almusabi, S.; Amna, T. Manganese Ferrite–Hydroxyapatite Nanocomposite Synthesis: Biogenic Waste Remodeling for Water Decontamination. *Nanomaterials* **2022**, *12*, 1631. [[CrossRef](#)]
2. Marimuthu, S.; Antonisamy, A.J.; Malayandi, S.; Rajendran, K.; Tsai, P.-C.; Pugazhendhi, A.; Ponnusamy, V.K. Silver nanoparticles in dye effluent treatment: A review on synthesis, treatment methods, mechanisms, photocatalytic degradation, toxic effects and mitigation of toxicity. *J. Photochem. Photobiol. B Biol.* **2020**, *205*, 111823. [[CrossRef](#)] [[PubMed](#)]
3. Inwati, G.K.; Yadav, V.K.; Ali, I.H.; Vuggili, S.B.; Kakodiya, S.D.; Solanki, M.K.; Yadav, K.K.; Ahn, Y.; Yadav, S.; Islam, S.; et al. 2D Personality of Multifunctional Carbon Nitrides towards Enhanced Catalytic Performance in Energy Storage and Remediation. *Appl. Sci.* **2022**, *12*, 3753. [[CrossRef](#)]
4. Rajendran, S.; Inwati, G.K.; Yadav, V.K.; Choudhary, N.; Solanki, M.B.; Abdellattif, M.H.; Yadav, K.K.; Gupta, N.; Islam, S.; Jeon, B.-H. Enriched Catalytic Activity of TiO₂ Nanoparticles Supported by Activated Carbon for Noxious Pollutant Elimination. *Nanomaterials* **2021**, *11*, 2808. [[CrossRef](#)] [[PubMed](#)]
5. Yadav, V.K.; Suriyaprabha, R.; Inwati, G.K.; Gupta, N.; Singh, B.; Lal, C.; Kumar, P.; Godha, M.; Kalasariya, H. A Noble and Economical Method for the Synthesis of Low Cost Zeolites From Coal Fly Ash Waste. *Adv. Mater. Process. Technol.* **2021**, 1–19. [[CrossRef](#)]
6. Inwati, G.K.; Kumar, P.; Roos, W.; Swart, H. Thermally induced structural metamorphosis of ZnO:Rb nanostructures for antibacterial impacts. *Colloids Surf. B Biointerfaces* **2020**, *188*, 110821. [[CrossRef](#)]
7. Kumar, P.; Mathpal, M.C.; Inwati, G.; Ghosh, S.; Kumar, V.; Roos, W.; Swart, H. Optical and surface properties of Zn doped CdO nanorods and antimicrobial applications. *Colloids Surf. A Physicochem. Eng. Asp.* **2020**, *605*, 125369. [[CrossRef](#)]
8. Kumar, P.; Inwati, G.K.; Mathpal, M.C.; Maze, J.; Swart, H.C. Recent advances on ferrites nanomaterial's as photocatalyst for environment. In *Advances in Nanostructured Materials*; Springer: Berlin/Heidelberg, Germany, 2022; pp. 381–409.
9. Inwati, G.; Kumar, P.; Roos, W.; Swart, H.; Singh, M. UV-irradiation effects on tuning LSPR of Cu/Ag nanoclusters in ion exchanged glass matrix and its thermodynamic behaviour. *J. Alloy. Compd.* **2020**, *823*, 153820. [[CrossRef](#)]
10. Padnya, P.; Gorbachuk, V.; Stoikov, I. The role of calix[n]arenes and pillar[n]arenes in the design of silver nanoparticles: Self-assembly and application. *Int. J. Mol. Sci.* **2020**, *21*, 1425. [[CrossRef](#)]
11. Batool, M.; Daoush, W.M.; Hussain, M.K. Dye Sequestration Using Biosynthesized Silver Nanoparticles Adsorbent in Aqueous Solutions. *Crystals* **2022**, *12*, 662. [[CrossRef](#)]
12. Rozhin, A.; Batasheva, S.; Kruchkova, M.; Cherednichenko, Y.; Rozhina, E.; Fakhrullin, R. Biogenic Silver Nanoparticles: Synthesis and Application as Antibacterial and Antifungal Agents. *Micromachines* **2021**, *12*, 1480. [[CrossRef](#)] [[PubMed](#)]
13. Thian, E.S.; Lim, P.; Shi, Z.; Tay, B.; Neoh, K. Silver-Doped Apatite as a Bioactive and an Antimicrobial Bone Material. *Key Eng. Mater.* **2012**, *493–494*, 27–30. [[CrossRef](#)]

14. Modi, S.; Inwati, G.K.; Gacem, A.; Abullais, S.S.; Prajapati, R.; Yadav, V.K.; Syed, R.; Alqahtani, M.S.; Yadav, K.K.; Islam, S.; et al. Nanostructured Antibiotics and Their Emerging Medicinal Applications: An Overview of Nanoantibiotics. *Antibiotics* **2022**, *11*, 708. [[CrossRef](#)] [[PubMed](#)]
15. Andrade, F.A.C.; Vercik, L.C.D.O.; Monteiro, F.J.; Rigo, E.C.D.S. Preparation, characterization and antibacterial properties of silver nanoparticles–hydroxyapatite composites by a simple and eco-friendly method. *Ceram. Int.* **2016**, *42*, 2271–2280. [[CrossRef](#)]
16. Fihri, A.; Len, C.; Varma, R.S.; Solhy, A. Hydroxyapatite: A review of syntheses, structure and applications in heterogeneous catalysis. *Coord. Chem. Rev.* **2017**, *347*, 48–76. [[CrossRef](#)]
17. Pai, S.; Kini, S.M.; Selvaraj, R.; Pugazhendhi, A. A review on the synthesis of hydroxyapatite, its composites and adsorptive removal of pollutants from wastewater. *J. Water Process Eng.* **2020**, *38*, 101574. [[CrossRef](#)]
18. Vijayaraghavan, P.; Rathi, M.; Almaary, K.S.; Alkhattaf, F.S.; Elbadawi, Y.B.; Chang, S.W.; Ravindran, B. Preparation and antibacterial application of hydroxyapatite doped Silver nanoparticles derived from chicken bone. *J. King Saud Univ. Sci.* **2022**, *34*, 101749. [[CrossRef](#)]
19. Inwati, G.; Rao, Y.; Singh, M. Thermodynamically induced in Situ and Tunable Cu Plasmonic Behaviour. *Sci. Rep.* **2018**, *8*, 3006. [[CrossRef](#)]
20. Gnanamoorthy, G.; Kumar Yadav, V.; Ali, D.; Ramar, K.; Gokhlesh Kumar Narayanan, V. New designing (NH₄)₂SiP₄O₁₃ nanowires and effective photocatalytic degradation of Malachite green and antimicrobial properties. *Chem. Phys. Lett.* **2022**, *803*, 139817. [[CrossRef](#)]
21. Malik, P.; Inwati, G.K.; Mukherjee, T.K.; Singh, S.; Singh, M. Green silver nanoparticle and Tween-20 modulated pro-oxidant to antioxidant curcumin transformation in aqueous CTAB stabilized peanut oil emulsions. *J. Mol. Liq.* **2019**, *291*, 111252. [[CrossRef](#)]
22. Nguyen, V.P.; Le Trung, H.; Nguyen, T.H.; Hoang, D.; Tran, T.H. Synthesis of Biogenic Silver Nanoparticles with Eco-Friendly Processes Using Ganoderma lucidum Extract and Evaluation of Their Theranostic Applications. *J. Nanomater.* **2021**, *2021*, 6135920. [[CrossRef](#)]
23. Jadalannagari, S.; Deshmukh, K.; Ramanan, S.R.; Kowshik, M. Antimicrobial activity of hemocompatible silver doped hydroxyapatite nanoparticles synthesized by modified sol–gel technique. *Appl. Nanosci.* **2014**, *4*, 133–141. [[CrossRef](#)]
24. Ciobanu, C.S.; Iconaru, S.L.; Le Coustumer, P.; Constantin, L.V.; Predoi, D. Antibacterial activity of silver-doped hydroxyapatite nanoparticles against gram-positive and gram-negative bacteria. *Nanoscale Res. Lett.* **2012**, *7*, 324. [[CrossRef](#)] [[PubMed](#)]
25. Inwati, G.; Rao, Y.; Singh, M. In Situ Growth of Low-Dimensional Silver Nanoclusters with Their Tunable Plasmonic and Thermodynamic Behavior. *ACS Omega* **2017**, *2*, 5748–5758. [[CrossRef](#)] [[PubMed](#)]
26. Ciobanu, C.S.; Iconaru, S.L.; Chifiriuc, M.C.; Costescu, A.; Le Coustumer, P.; Predoi, D. Synthesis and Antimicrobial Activity of Silver-Doped Hydroxyapatite Nanoparticles. *BioMed Res. Int.* **2013**, *2013*, 916218. [[CrossRef](#)]
27. Inwati, G.K.; Kumar, P.; Singh, M.; Yadav, V.K.; Kumar, A.; Soma, V.R.; Swart, H. Study of photoluminescence and nonlinear optical behaviour of AgCu nanoparticles for nanophotonics. *Nano-Struct. Nano-Objects* **2021**, *28*, 100807. [[CrossRef](#)]
28. Wei, W.; Yang, L.; Zhong, W.H.; Li, S.Y.; Cui, J.; Wei, Z.G. Fast removal of methylene blue from aqueous solution by adsorption onto poorly crystalline hydroxyapatite nanoparticles. *Dig. J. Nanomater. Biostructures* **2015**, *10*, 1343–1363.
29. Banerjee, S.; Bagchi, B.; Bhandary, S.; Kool, A.; Hoque, N.A.; Thakur, P.; Das, S. A facile vacuum assisted synthesis of nanoparticle impregnated hydroxyapatite composites having excellent antimicrobial properties and biocompatibility. *Ceram. Int.* **2018**, *44*, 1066–1077. [[CrossRef](#)]
30. Piccirillo, C.; Castro, P. Calcium hydroxyapatite-based photocatalysts for environment remediation: Characteristics, performances and future perspectives. *J. Environ. Manag.* **2017**, *193*, 79–91. [[CrossRef](#)]
31. Narendran, P.; Rajendran, A.; Garhnyak, M.; Garhnyak, L.; Nivedhitha, J.; Devi, C.; Pattanayak, D.K. Influence of pH on wet-synthesis of silver decorated hydroxyapatite nanopowder. *Colloids Surf. B Biointerfaces* **2018**, *169*, 143–150. [[CrossRef](#)]
32. Ahmad, M.; Ahmad, I.; Ahmed, E.; Akhtar, M.S.; Khalid, N. Facile and inexpensive synthesis of Ag doped ZnO/CNTs composite: Study on the efficient photocatalytic activity and photocatalytic mechanism. *J. Mol. Liq.* **2020**, *311*, 113326. [[CrossRef](#)]
33. Kumar, P.; Mathpal, M.C.; Inwati, G.K.; Swart, H.C.; Roos, W. Graphene oxide based semiconducting nanomaterial's composites for environmental applications. In *Nanoscale Compound Semiconductors and Their Optoelectronics Applications*; Woodhead Publishing: Cambridge, UK, 2022; pp. 407–431.
34. Inwati, G.K.; Kumar, P.; Swart, H.C. Multifunctional properties of hybrid semiconducting nanomaterials and their applications. In *Nanoscale Compound Semiconductors and their Optoelectronics Applications*; Woodhead Publishing: Cambridge, UK, 2022; pp. 315–350.
35. Modi, S.; Prajapati, R.; Inwati, G.K.; Deepa, N.; Tirth, V.; Yadav, V.K.; Yadav, K.K.; Islam, S.; Gupta, P.; Kim, D.-H.; et al. Recent Trends in Fascinating Applications of Nanotechnology in Allied Health Sciences. *Crystals* **2021**, *12*, 39. [[CrossRef](#)]
36. Yadav, V.K.; Choudhary, N.; Khan, S.H.; Malik, P.; Inwati, G.K.; Suriyaprabha, R.; Ravi, R.K. Synthesis and characterisation of nano-biosorbents and their applications for waste water treatment. In *Handbook of Research on Emerging Developments and Environmental Impacts of Ecological Chemistry*; Gheorghe, D., Ashok, V., Eds.; IGI Global: Hershey, PA, USA, 2020; pp. 252–290.
37. Kumar, P.; Mathpal, M.C.; Ghosh, S.; Inwati, G.K.; Maze, J.R.; Duvenhage, M.-M.; Roos, W.; Swart, H. Plasmonic Au nanoparticles embedded in glass: Study of TOF-SIMS, XPS and its enhanced antimicrobial activities. *J. Alloys Compd.* **2022**, *909*, 164789. [[CrossRef](#)]
38. Kumar, N.; Inwati, G.K.; Ahmed, E.M.; Lal, C.; Makwana, B.; Yadav, V.K.; Islam, S.; Ahn, H.-J.; Yadav, K.K.; Jeon, B.-H. Modified 7-Chloro-11H-indeno[1,2-b]quinoxaline Heterocyclic System for Biological Activities. *Catalysts* **2022**, *12*, 213. [[CrossRef](#)]